

Fully spin-dependent transport of triangular graphene flakes

Tomoya Ono¹, Tadashi Ota¹, and Yoshiyuki Egami²

¹*Department of Precision Science and Technology,*

Osaka University, Suita, Osaka 565-0871, Japan

²*Nagasaki University Advanced Computing Center,*

Nagasaki University, Bunkyo-machi, Nagasaki 852-8521, Japan

(Dated: March 15, 2019)

Abstract

The magnetic moment and spin-polarized electron transport properties of triangular graphene flakes surrounded by boron nitride sheets (BNC structures) are studied by using first-principles calculations based on density functional theory. Their dependence on the BNC structure is discussed, revealing that small isolated graphene flakes have large magnetic moment. When the BNC structure is suspended between graphene electrodes, the spin-polarized charge density distribution accumulates at the edge of the graphene flakes and no spin polarization is observed in the graphene electrodes. We also found that the BNC structure demonstrates perfectly spin-polarized transport properties in the wide energy window around the Fermi level. Our first-principles results indicate that the BNC structure provides new possibilities to electrically control spin.

PACS numbers: 72.80.Vp, 73.21.-b, 75.75.-c, 85.75.Mm

9 I. INTRODUCTION

10 Graphene,¹ as a two-dimensional monolayer honeycomb structure of carbon, is known to
11 exhibit a rich variety of electronic structures and is expected to be one of the most promis-
12 ing new materials for future nanoelectronics. The electronic reconstruction of graphenes
13 induced at boundaries can give rise to metal or insulator states,² magnetism,³ or even
14 superconductivity.⁴ The discovery of zigzag graphene nanoribbons,^{3,5} in which an opposite
15 spin orientation crosses the ribbon between ferromagnetically ordered edge states on each
16 edge, through theoretical calculations has attracted a great deal of interest^{6,7} in spintron-
17 ics applications based on graphene based materials. The possibility of controlling electron
18 transport by means of the spin degree of freedom has recently attracted attention, because
19 spintronics devices may have potential for applications in future commercial electronics, and
20 generate insights into the fundamental properties of electron spin physics in solids. From the
21 viewpoint of the development of highly efficient spintronics devices, spin-filter effect, which
22 can be used for efficient injection of spins into magnetic junctions, is an important issue of
23 concern and debate. Okada and Oshiyama⁸ studied the spin polarizations of two dimen-
24 sional structures composed of boron, nitrogen, and carbon, in which triangular graphene
25 flakes is surrounded by boron nitride (BN) sheets (referred to as BNC structures after this),
26 through first-principles calculations and found that flat-band states can be observed around
27 the Fermi level and the BNC structures are ferromagnetically polarized. Zheng *et al.*⁹ ex-
28 amined the spin transport properties of graphene antidots, i.e., graphenes with rectangular
29 or triangular holes, and observed the spin polarization of electron current in the triangular
30 antidots. However the energy window where current is perfectly spin polarized is quite small
31 in their system because the energy of the edge states contributing to spin-polarized current
32 does not shift significantly around the antidots.

33 We study the relationship between the magnetic moment of the BNC structures and their
34 sizes. The spin-dependent transport properties of graphene/BNC/graphene (G/BNC/G)
35 structures, where the BNC structures are sandwiched with graphene electrodes, are also
36 examined. We found that small isolated graphene flakes exhibits large magnetic moment
37 and BNC structures with the small flakes demonstrate fully spin-polarized current with a
38 large energy range of incident electrons.

39 All calculations are done within the framework of density functional theory (DFT)¹⁰

using a real-space finite-difference approach,^{11,12} which makes it possible to carry out calculations with a high degree of accuracy by combining them with a timesaving double-grid technique.^{12,13} Valence electron-ion interaction is described by using norm-conserving pseudopotentials¹⁴ generated using the scheme proposed by Troullier and Martins.¹⁵ Exchange and correlation effects are treated within the local spin density approximation¹⁶ of DFT.

II. RESULTS AND DISCUSSION

A. magnetic moment of graphene flakes

Let us first consider three periodic BNC structures to investigate what effect the size of carbon regions has on the magnetic moment. Figures 1(a), 1(b), and 1(c) show the computational models we employed here. There are 64 atoms in the supercell. Periodic boundary conditions are imposed on all directions and a repeating sheet model is separated by 9.0 Å in each layer for all the calculations presented in this section. The Brillouin zone is sampled by a four k -point grid. The lattice constant of graphene is set at 1.41 Å with a real-space grid spacing of ~ 0.18 Å and structural optimization has been performed until the remaining forces are less than 5 mRy/Å. The calculated magnetic moments of the BNC structures are listed in Table I. The magnetic moment of the BNC structure with small BN segments is much smaller than that expected from Lieb's theorem in the biparticle lattice, which is proved in the Hubbard model ($S_0=2$)¹⁷ due to the interaction between graphene flakes in the neighboring supercell. The BNC structures with the smallest graphene flakes are found to exhibit the largest magnetic moments that approach those expected from Lieb's theorem as the graphene flakes are isolated. We then examine variations in the magnetic moments as a function of the distance in the z direction between graphene flakes in the neighboring supercell. Figures 2(a), 2(b), and 2(c) show the calculated atomic configurations. Integration over the Brillouin zone is carried out using an eight k -point grid. From Table I, we can see the magnetic moment increases with the increment in the graphene-flake distance and model (c) in Fig. 2 with the long graphene-flake distance emerges the largest magnetic moment. Figures 1 and 2 also show the calculated spin densities, $n_{\uparrow}(r) - n_{\downarrow}(r)$, of the BNC structures. One can see that magnetic ordering appears on the

edge of the graphene flakes and magnetic moment is strengthened when the electrons around the graphene flakes are localized by the insulating behavior of the BN regions.

B. Magnetic moment of G/BNC/G structure

Graphene is one of the best candidates for buffer layers between BNC structures and electrodes because of its metallic characteristics and long-lived spin coherence. We explored the magnetic moment of BNC structures connected to graphene (G/BNC/G structures). Since the transition from ferromagnetic to nonmagnetic states occurs when fewer than 0.05 electrons are doped per BNC structure and the existence of an optimum width for the BN region has been given,⁸ it is of interest whether ferromagnetic states can still be observed in G/BNC/G structures. When primary importance is attached to the magnetic moment of BNC structures, a wider BN region is necessary to obtain large magnetic moment. However, in terms of the transmission of electrons, a wider BN region acting as an insulator could be an obstacle to obtaining larger conductance. The computational model is outlined in Fig. 3. The integration over the Brillouin zone for the x direction is carried out by equidistant sampling of the four k -point grid. The calculated total magnetic moment is found to be $1.51 \mu_B/\text{cell}$. The magnetic behavior is illustrated by plotting contours of the difference in the charge density distributions on the plane in Fig. 3. Note that the spin polarization accumulates in the BNC regions and the graphene structures as the electrodes do not exhibit magnetic ordering.

C. Transport properties of G/BNC/G structure

It is important to evaluate quantitative spin transmissions toward the application of spin-filter materials. Based on the results in the previous subsection, the spin-transport properties of the model in Fig. 3 are investigated. We establish a computational model for the transport calculations, where the G/BNC/G structure is sandwiched between the electrodes. The scattering wave functions of the electrons propagating from the left electrode are determined to include the rest of the semi-infinite electrodes by solving the following

95 simultaneous equations for each incident wave function $\Phi_L^{in}(z_k)$:

$$\begin{bmatrix} E - \hat{H}_T - \hat{H}_\Sigma \end{bmatrix} \begin{bmatrix} \Psi(z_0) \\ \Psi(z_1) \\ \vdots \\ \Psi(z_{N_z+1}) \end{bmatrix} = \begin{bmatrix} B_z^\dagger \Phi_L^{in}(z_{-1}) - \Sigma_L^r(z_0) \Phi_L^{in}(z_0) \\ 0 \\ \vdots \\ 0 \end{bmatrix}. \quad (1)$$

96 Here, \hat{H}_T is the truncated part of the Hamiltonian of the scattering region and E is the energy
 97 of the incident electrons. The $\Psi(z_i)$ is the set of values of the scattering wave function on
 98 the x - y plane at $z = z_i$ and it satisfies the scattering boundary condition, i.e.,

$$\Psi(z_k) = \begin{cases} \Phi_L^{in}(z_k) + \sum_{i=1}^{N_x N_y} r_i \Phi_i^{ref}(z_k) & (k \leq 0) \\ \sum_{i=1}^{N_x N_y} t_i \Phi_i^{tra}(z_k) & (k \geq N_z + 1) \end{cases}, \quad (2)$$

99 where r_i (t_i) is the reflection (transmission) coefficient, $\Phi_i^{ref}(z_k)$ ($\Phi_i^{tra}(z_k)$) is the generalized
 100 Bloch state in semi-infinite electrodes for reflected (transmitted) electrons, N_x , N_y , and N_z
 101 are the numbers of grid points in x , y , and z directions, respectively. In addition, \hat{H}_Σ is a
 102 zero matrix except that the first and the last elements are the retarded self-energy matrices
 103 in the left and right electrodes, $\Sigma_L^r(z_0)$ and $\Sigma_R^r(z_{N_z+1})$, respectively. Further details can
 104 be found in Refs. 18, 19, and 20. The retarded self-energy matrices for copper jellium are
 105 employed and sufficiently long graphene buffer layers (eight layers) are inserted between the
 106 BNC structure and electrodes to suppress the unfavorable effects of the copper electrodes.
 107 The distance between the edge atoms of the graphene and the jellium electrode is set at
 108 0.38 Å and a grid spacing of 0.27 Å is employed. The scattering wave functions from the
 109 right electrode are treated in the same way. We first calculate \hat{H}_T using periodic boundary
 110 conditions and then compute the scattering wave functions obtained non-self-consistently.
 111 It has been reported that this procedure is just as accurate in the linear response regime but
 112 significantly more efficient than being self-consistent on a scattering basis.²¹ The Brillouin
 113 zone is sampled with the four k -point grid to set up \hat{H}_T while a twenty k -point grid is used
 114 for the transport calculations. The conductance per unit cell under zero temperature and
 115 zero bias is described by the Landauer-Büttiker formula,²²

$$G(E) = G_0 \int d\mathbf{k}_\parallel \frac{A}{(2\pi)^2} \text{Tr}(\mathbf{T}^\dagger \mathbf{T}), \quad (3)$$

where \mathbf{T} is a transmission-coefficient matrix, A is the area of the unit cell in the x and y directions, and $G_0 = 2e^2/h$ with e and h being the electron charge and Plank's constant, respectively.

Figure 4 plots the conductance of G/BNC/G structures as a function of the energy of the incident electrons. Although BN sheets are insulators, considerable electron transmission through BNC structures can be observed. There is significant spin-polarized electron current observed that can be associated with the BNC structures. Here, we have defined parameter $P(E) = [\sigma_{\uparrow}(E) - \sigma_{\downarrow}(E)]/[\sigma_{\uparrow}(E) + \sigma_{\downarrow}(E)]$ to characterize the spin polarization of electron current, where the conductance of spin $s(=\uparrow, \downarrow)$ is donated by $\sigma_s(E)$. The spin-polarization ratio is found to be ~ 1 , which is comparable to that obtained with ferromagnetic tunnel junctions using transition metal.²³ The peaks of the conductance of the up-spin and down-spin channels are split by 0.5 eV. Moreover, the energy ranges of $P(E) = 1$ and those of $P(E) = -1$ are completely separated. Although graphene is a gapless semiconductor, conductance of the up spin (down spin) is negligibly small except for the energy ranges of $P(E) = 1$ ($P(E) = -1$) because of the finite size effect of the BNC structure. This means that we can control spin-polarized current by tuning gate bias.

Figure 5 shows the energy band structure of the BNC structure in Fig. 2(b) and the local density of state (LDOS) of the G/BNC/G structures, which have been plotted by integrating them along the x - y plane, $\rho(z, E) = \int |\psi(\mathbf{r}, E)|^2 d\mathbf{r}_{\parallel}$, where $\mathbf{r} = (x, y, z)$, ψ is the wave function and E is the energy of the states. The states of up-spin electrons have shifted to lower energy and those of down-spin electrons have been shifted to higher energy in the BNC structure although the spin polarization is negligibly small in the LDOS of the graphene region. Thus, the conductance spectrum of the BNC structure is not symmetric around the Fermi level whereas that for graphene is symmetric. Moreover, the difference in energy between these states of up-spin and down-spin electrons is 0.5 eV. We can see the good correspondence between conductance and LDOS, which implies that the electronic structure of the BNC structure contributes to the spin-polarized electron current.

The charge density distribution of scattering waves for incident electrons from the left electrode has been shown in Fig. 6. There are two edge states around the Fermi level in the BNC structure in Fig. 5; the charge density distribution of one edge state is parallel to the base of the triangular graphene flake and that of the other edge state is parallel to the leg. As seen in Fig. 6, the former edge state contributes to electron transport at a lower energy

range and the latter contributes at higher energy in both spin channels.

Such a spintronic device can be compared to another theoretical proposal that achieves spin-filter material. Compared with the graphene antidot system,⁹ this BNC structure has a wider energy window where the current is fully polarized. The inserted BN segment between the graphene flakes and electrodes insulates the edge state so that the edge states accumulate in the graphene flakes, which results in a higher magnetic moment for the BNC structure. Our results indicate that the BNC structure is one of the most promising candidates for electronic control over spin transport.

III. SUMMARY

We investigated the electronic structures and transport properties of triangular graphene flakes surrounded by BN sheets using first-principles calculations. We found that the magnetic moment of the graphene flakes increases as the flakes become small and as they become isolated. When the BNC structure is connected to graphene electrodes, the spin polarization of the charge density distribution accumulates at the edges of the flakes and no spin polarizations are observed in the graphene electrodes. First-principles transport calculation revealed that electron transport through the BNC structure is fully polarized in a wide energy range around the Fermi level. These results should stimulate interest in spin-transport devices using carbon-based materials and a bottom-up technology.

ACKNOWLEDGEMENTS

The authors would like to thank Kikuji Hirose and Yoshitada Morikawa of Osaka University for fruitful discussion. This research was partially supported by Strategic Japanese-German Cooperative Program from Japan Science and Technology Agency and Deutsche Forschungsgemeinschaft, by a Grant-in-Aid for Scientific Research on Innovative Areas (Grant No. 22104007) from the Ministry of Education, Culture, Sports, Science and Technology, Japan. The numerical calculation was carried out using the computer facilities of the Institute for Solid State Physics at the University of Tokyo, the Research Center for Computational Science at the National Institute of Natural Science, Center for Computational Sciences at University of Tsukuba, and the Information Synergy Center at Tohoku

-
- ¹ K.S. Novoselov, A.K. Geim, S.V. Morozov, D. Jiang, Y. Zhang, S.V. Dubonos, I.V. Grigorieva, and A.A. Firsov, *Science* **306**, 666 (2004).
- ² N. Hamada, S.I. Sawada, and A. Oshiyama, *Phys. Rev. Lett.* **68**, 1579 (1992).
- ³ M. Fujita, K. Wakabayashi, K. Nakada and K. Kusakabe, *J. Phys. Soc. Jpn.* **65**, 1920 (1996).
- ⁴ H.B. Heersche, P. Jarillo-Herrero, J.B. Oostinga, L.M.K. Vandersypen, and A.F. Morpurgo, *Nature* **446**, 56 (2007).
- ⁵ K. Nakada, M. Fujita, G. Dresselhaus, and M.S. Dresselhaus, *Phys. Rev. B* **54**, 17954 (1996).
- ⁶ N. Tombros, C. Jozsa, M. Popinciuc, H.T. Jonkman, and B.J. van Wees, *Nature* **448**, 571 (2007).
- ⁷ V.M. Karpan, G. Giovannetti, P.A. Khomyakov, M. Talanana, A.A. Starikov, M. Zwierzycki, J. van den Brink, G. Brocks, and P.J. Kelly, *Phys. Rev. Lett.* **99**, 176602 (2007).
- ⁸ S. Okada and A. Oshiyama, *Phys. Rev. Lett.* **87**, 146803 (2001).
- ⁹ X.H. Zheng, G.R. Zhang, Z. Zeng, Víctor M. García-Suárez, and Colin J. Lambert, *Phys. Rev. B* **80**, 075413 (2009).
- ¹⁰ P. Hohenberg and W. Kohn, *Phys. Rev.* **136**, B864 (1964).
- ¹¹ J.R. Chelikowsky, N. Troullier, and Y. Saad, *Phys. Rev. Lett.* **72**, 1240 (1994)
- ¹² K. Hirose, T. Ono, Y. Fujimoto, and S. Tsukamoto, *First Principles Calculations in Real-Space Formalism, Electronic Configurations and Transport Properties of Nanostructures* (Imperial College, London, 2005).
- ¹³ T. Ono and K. Hirose, *Phys. Rev. Lett.* **82**, 5016 (1999); *Phys. Rev. B* **72**, 085115 (2005).
- ¹⁴ We used the norm-conserving pseudopotentials NCPS97 constructed by K. Kobayashi. See K. Kobayashi, *Comput. Mater. Sci.* **14**, 72 (1999).
- ¹⁵ N. Troullier and J. L. Martins, *Phys. Rev. B* **43**, 1993 (1991).
- ¹⁶ J. P. Perdew and A. Zunger, *Phys. Rev. B* **23**, 5048 (1981).
- ¹⁷ E.H. Lieb, *Phys. Rev. Lett.* **62**, 1201 (1989).
- ¹⁸ Y. Fujimoto and K. Hirose, *Phys. Rev. B* **67**, 195315 (2003).
- ¹⁹ L. Kong, M.L. Tiago, and J.R. Chelikowsky, *Phys. Rev. B* **73**, 195118 (2006).
- ²⁰ Y. Egami, K. Hirose, and T. Ono, *Phys. Rev. E* **82**, 056706 (2010).

- ²¹ L. Kong, J.R. Chelikowsky, J.B. Neaton, and Steven G. Louie, Phys. Rev. B **76**, 235422 (2007).
- ²² M. Büttiker, Y. Imry, R. Landauer, and S. Pinhas, Phys. Rev. B **31**, 6207 (1985).
- ²³ S. Kokado, N. Fujima, K. Harigaya, H. Shimizu, and A. Sakuma, Phys. Rev. B **73**, 172410 (2006).

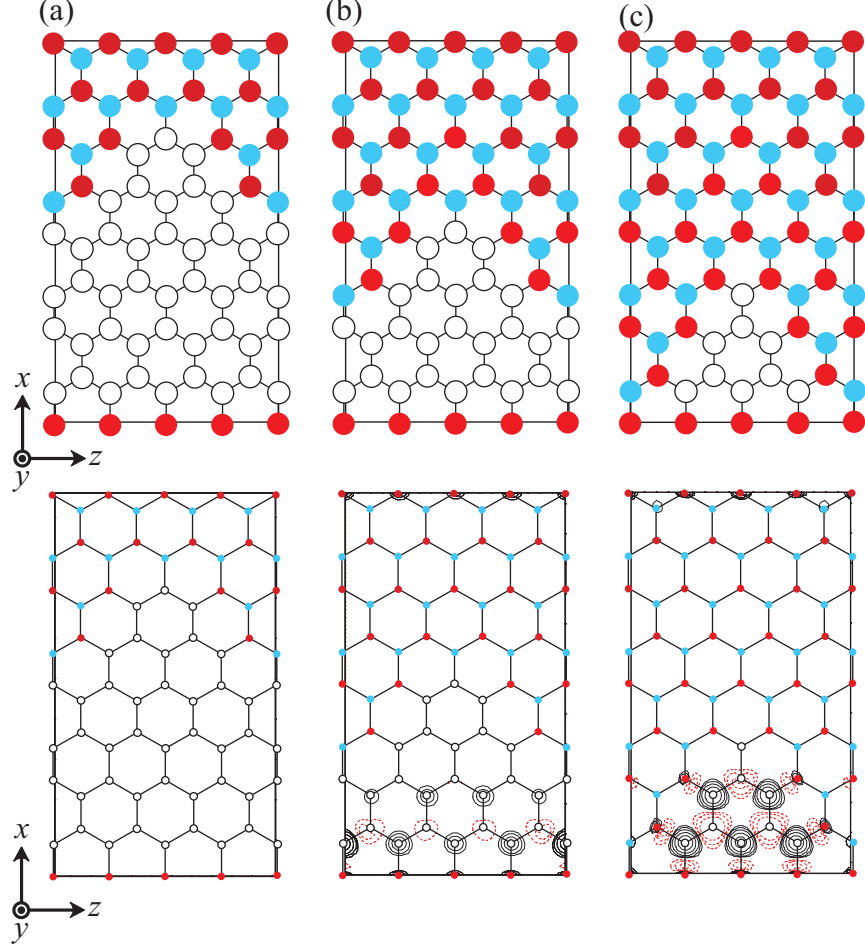


FIG. 1. (color online) Top view of computational models (top panel) and contour plots of difference between up-spin and down-spin charge density distributions (bottom panel). (a) Represents large graphene flake model, (b) represents medium graphene flake model, and (c) represents small graphene flake model. White, light blue (gray), and red (black) circles correspond to C, B, and N atoms. Positive values of spin density are indicated by solid lines and negative by dashed lines. Each contour represents twice or half the density of adjacent contour lines. The lowest contour represents $3.29 \times 10^{-3} e/\text{\AA}^3$.

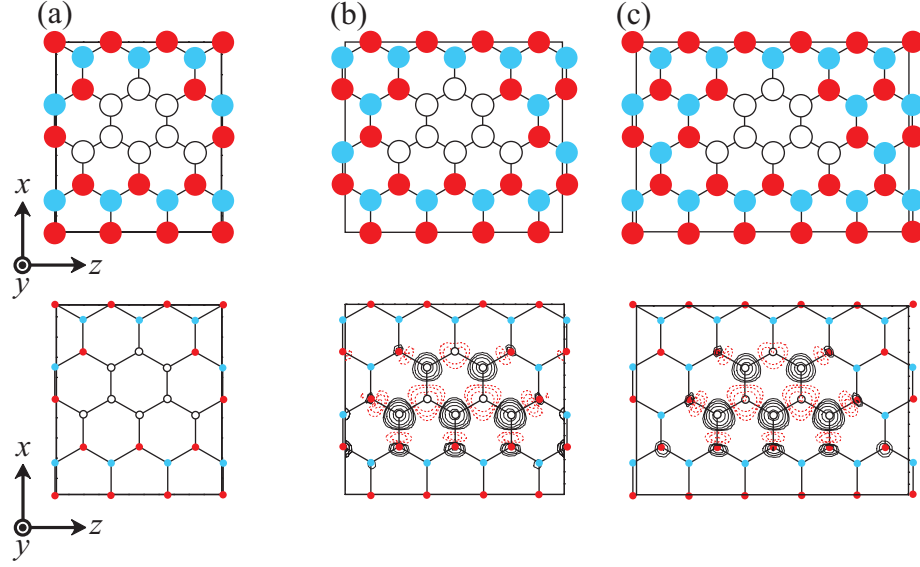


FIG. 2. (color online) Top view of computational models (top panel) and contour plots of difference between up-spin and down-spin charge density distributions (bottom panel). (a), (b), and (c) correspond to short, medium, and long distance between graphene flakes. The symbols have the same meanings as those in Fig. 1.

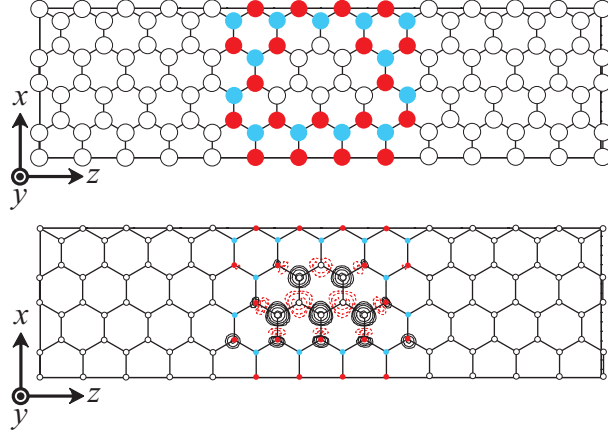


FIG. 3. (color online) Top view of computational models (top panel) and contour plots of difference between up-spin and down-spin charge density distributions (bottom panel). The symbols have the same meanings as those in Fig. 1.

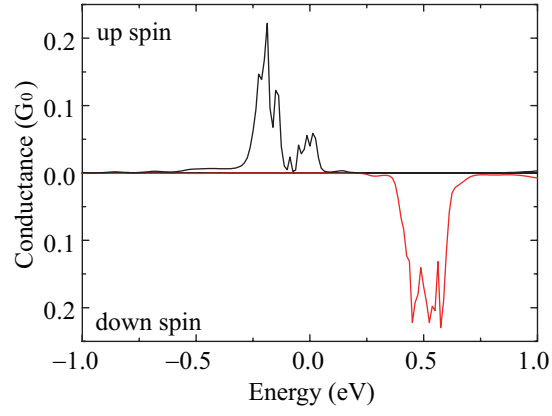


FIG. 4. Conductance as a function of energy of incident electrons. Zero energy is chosen to be at Fermi level.

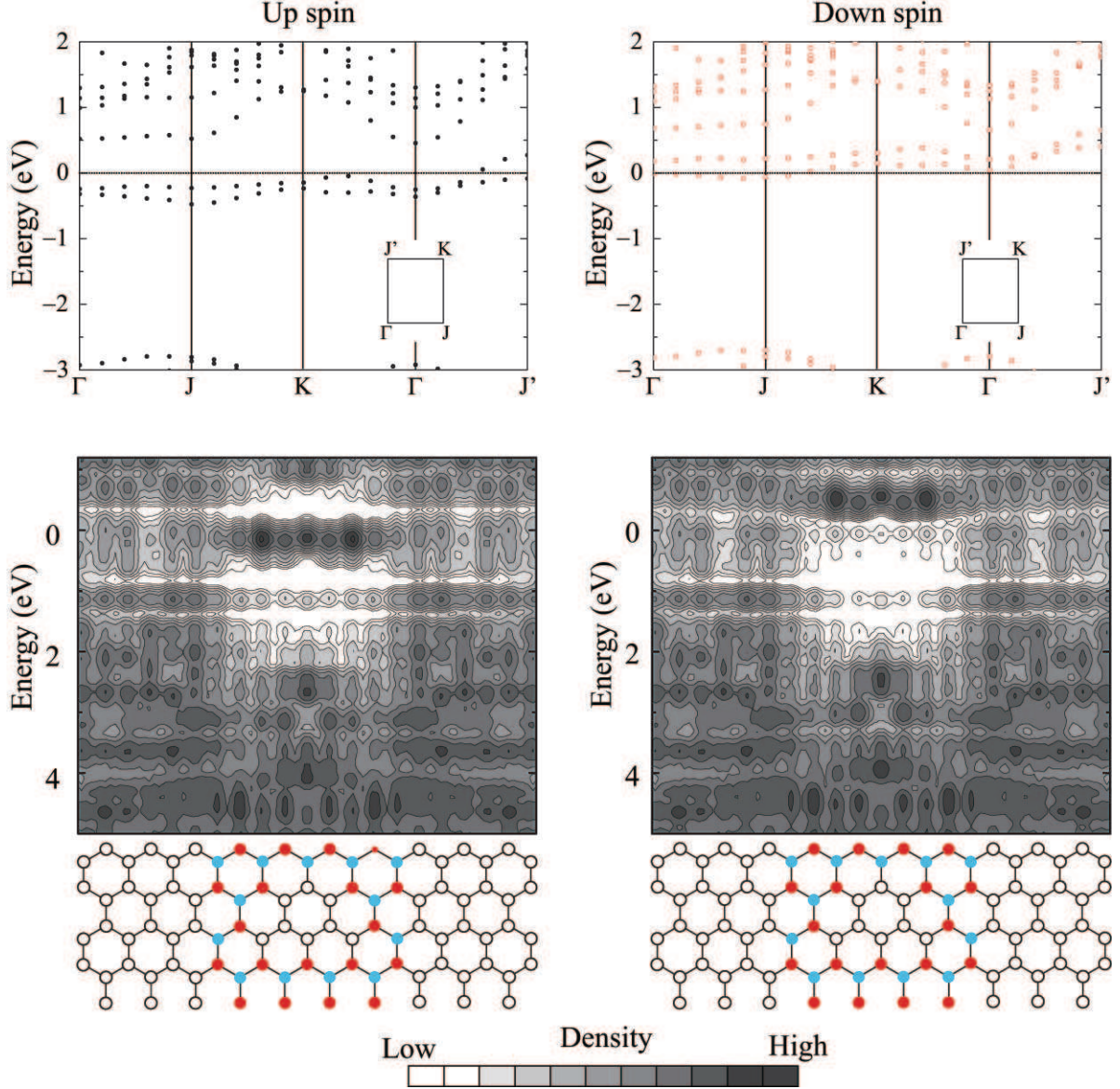


FIG. 5. (color online) Energy band structure of the BNC structure in Fig. 2(b) (top panel) and distributions of LDOS of the G/BNC/G structure integrated on plane parallel to interface as functions of relative energy from Fermi level (bottom panel). Zero energy is chosen to be at the Fermi level. Each contour represents twice or half the density of the adjacent contour lines, and the lowest contour is $6.78 \times 10^{-5} \text{ e/eV/\AA}$. The atomic configurations have been given as a visual guide below the graph and the symbols have the same meanings as those in Fig. 1.

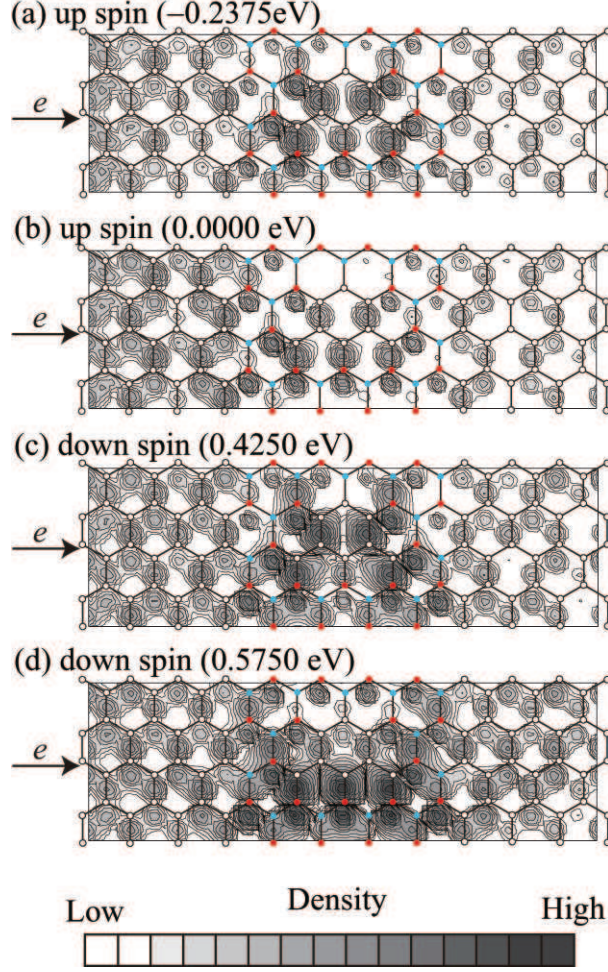


FIG. 6. Charge density distributions of scattering waves for incident electrons emitted from left electrode on plane parallel to BNC structure. Each contour represents twice or half the density of the adjacent contour lines, and the lowest contour is $3.10 \times 10^{-2} e/\text{\AA}^3$. The symbols have the same meanings as those in Fig. 1. Energies in parentheses have been counted from the Fermi level.

TABLE I. Calculated magnetic moments of BNC structures. 1(a), 1(b), 1(c), 2(a), 2(b), and 2(c) correspond to structures in Figs. 1 and 2.

Model	Magnetic moment (μ_B/cell)
1(a)	0.00
1(b)	0.64
1(c)	1.96
2(a)	0.00
2(b)	1.64
2(c)	1.65